SIMULATION OF THE UPWARD GOING FLUX OF THERMAL RADIATION SCATTERED BY AEROSOL

PART II. RADIUS OF THE ADJACENCY EFFECT

S.V. Afonin, V.V. Belov, and I.Yu. Makushkina

Institute of Atmospheric Optics,
Siberian Branch of the Russian Academy of Sciences, Tomsk
Received March 10, 1994

We consider spatial characteristics of the aerosol-scattered upward flux of thermal radiation emitted by the "atmosphere-underlying surface" system. The radius of lateral illumination effect is compared to spatial resolutions of satellite systems for IR remote sensing of the underlying surface.

1. INTRODUCTION

In our previous study[1] we presented results on the structure and intensity of the upward going flux of thermal radiation from the atmosphere and the underlying surface scattered by aerosol in the ranges 3.5–4 μm and 10.3–11.3 μm. In particular, it was demonstrated that the surface dominates in forming the intensity of such a radiation. Apparently, natural extension of these studies would be to investigate spatial characteristics important for description of the formation of that flux, i.e., the radius of lateral illumination (the adjacency effect)[2] that is the effective surface area, which one should take into account while calculating the radiative temperature $T_к$ of the "atmosphere-underlying surface" (A–US) system at a preset accuracy.

Below we analyze the estimated radii of lateral illumination due to the adjacency effect for various optical and geometric observational conditions within the accuracy range of 0.5–1.0° in radiative temperature. Choosing this range we aimed at applying such data to the problem of remote sensing of temperature of the underlying surface.

2. BASIC CHARACTERISTICS OF SIMULATION

In our previous study[1] we used the algorithm of direct simulation along the conjugated trajectories to calculate the flux intensity of scattered radiation J_λ^{MS} and separated the contributions from the underlying surface (J_{surf}^{MS}) and the atmosphere (J_{atm}^{MS}). The same algorithm was employed to estimate the values $J_{surf}^{MS}(R)$, formed by the underlying surface within the radius R.

Apparently, with R increasing, the value $J_{surf}^{MS}(R)$ tends to J_{surf}^{MS}. Along with these calculations we estimated the spatial characteristic

$$F(r) = \frac{1}{2\pi r}\frac{\partial J_{surf}^{MS}(r)}{\partial r},$$

where r is the range from the point of sensing.

The value $F(r)$ describes the spatial density of surface radiation scattered by aerosol and characterizes the contribution to radiation coming from a unit surface areas at the distance r from the point of sensing into the overall intensity of scattered radiation (the latter being normalized by J_{surf}^{MS}).

At a preset computational accuracy for radiative temperature ($\delta T_к$) the radius of lateral illumination was retrieved from the interpolational set of temperatures $T_\lambda(R)$. Our computational scheme assumes division of the underlying surface into circular areas of various radii at a step $\Delta R \sim 1$ km, their common center being at the point where the sight line intersects the underlying surface. The above step was chosen so that to ensure a satisfactory accuracy of determination of the radius of lateral illumination via linear interpolation of $T_\lambda(R)$ (not less than 100 m). Having computed the interpolation set $T_\lambda(R)$ and choosing the accuracy of computation of radiative temperature $0.1° \le \delta T_\lambda \le 1°$, one may then find the effective radius R of such a surface area using following condition

$$T_\lambda - T_\lambda(R) = \delta T_\lambda$$

in such a way as to provide the selected δT_λ level.

3. OPTICAL AND GEOMETRIC CONDITIONS USED IN SIMULATION

Simulation was carried out under the following optical and geometric observational conditions: spectral ranges of 3.55–3.95 μm (λ = 3.75 μm) and 10.3–11.3 μm (λ = 10.8 μm); angles of observation φ = 0 and 45°; altitude of observation of 800 km; meteorological models of the atmosphere included the tropics, midlatitudinal summer and winter, the arctic summer, and the standard US–1976 model; maritime, rural, and urban aerosol models were used (visibility range S_M = 2–50 km); a homogeneous Lambertian surface emitting as a black body within the temperature range T_S = 272.2–299.7 K presented the underlying surface. Both optical and meteorological models used are described and illustrated in Ref. 1.

4. SIMULATION RESULTS

Results of estimating the radius of lateral illumination are presented in Figs. 1–3 and Table I. Their analysis yields the following:

0235-6880/94/06 430-05 $02.00

1. The radius of lateral illumination monotonically grows with increasing computational accuracy of radiative temperature (Fig. 1). As δT_k varies within 1–0.5°, this radius increases no more than by 2 km, while for δT_λ = 0.5–0.1° the variability range of R noticeably expands due to variations in the optical and meteorological parameters of the atmosphere.

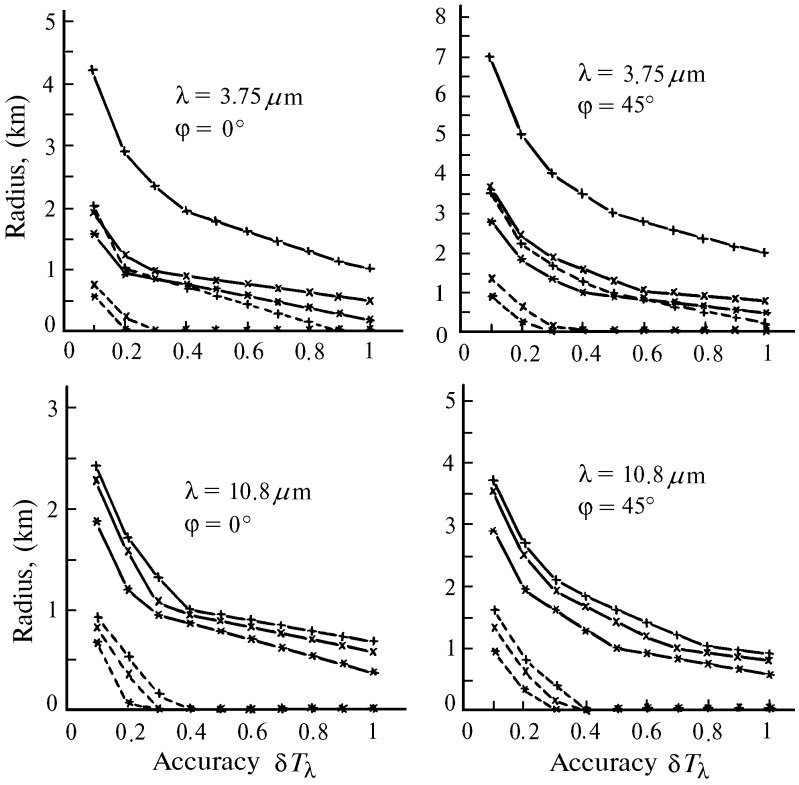

Fig. 1. Lateral illumination radius vs. computational accuracy of radiative temperature (midlatitudinal summer): rural (x), *maritime* (+), *and urban aerosol* (∗) *for* S_M = 2 (*solid line*) *and* 23 km (*dashed line*).

TABLE I. Maximum values of the radius of lateral illumination and the range of its maximum seasonal variations (the case of multiple scattering).

Aerosol type	S_M, km	φ = 0° accuracy (δT_k)			φ = 45° accuracy (δT_k)		
		1	0.5	0.1	1	0.5	0.1
λ = 3.75 μm							
maritime	2	1.823	2.730	6.036	3.013	4.417	8.808
	5	1.119	1.881	5.033	2.370	3.697	8.906
	10	0.891	1.467	4.032	1.774	2.902	8.086
	23	0.492	0.887	2.868	0.853	1.816	5.834
	variation range	0.317	0.555	1.252	0.604	0.874	2.554
rural	2	0.840	0.991	2.900	1.393	2.152	6.019
	5	0.497	0.830	1.987	0.817	1.469	4.464
	10	0.001	0.582	1.623	0.373	0.917	3.406
	23	0.001	0.001	0.966	0.001	0.186	2.175
	variation range	0.080	0.091	0.367	0.275	0.304	1.432
urban	2	0.668	0.896	1.992	0.855	1.401	3.442
	5	0.216	0.680	1.658	0.497	0.917	2.973
	10	0.001	0.329	1.188	0.001	0.644	2.476
	23	0.001	0.001	0.848	0.001	0.001	1.634
	variation range	0.075	0.090	0.244	0.142	0.144	0.437

TABLE I continued.

		λ = 10.8 μm					
maritime	2	1.280	1.943	4.736	2.315	3.518	8.120
	5	0.853	1.352	3.564	1.593	2.570	7.096
	10	0.555	0.925	2.778	0.935	1.849	5.656
	23	0.001	0.400	1.937	0.001	0.912	3.881
	variation range	0.408	0.896	2.224	1.246	1.712	4.794
rural	2	0.966	1.685	3.962	1.856	2.837	6.886
	5	0.714	0.982	2.986	1.114	1.971	5.856
	10	0.306	0.797	2.377	0.693	1.476	4.884
	23	0.001	0.046	1.604	0.001	0.545	3.084
	variation range	0.287	0.650	1.632	0.889	1.233	3.828
urban	2	0.860	1.186	2.958	1.395	2.043	4.894
	5	0.530	0.877	2.349	0.838	1.576	4.389
	10	0.001	0.635	1.926	0.402	0.979	3.777
	23	0.001	0.001	0.990	0.001	0.133	2.454
	variation range	0.338	0.349	1.079	0.608	0.941	2.294

2. For all the considered optical and meteorological situations the radius of lateral illumination monotonically increases with increasing optical thickness of aerosol τ_{sct} (Fig 2*a*). However, at low visibilities ($S_M < 10$ km) the rate at which that radius expands significantly slows down. Indeed, an increase of the optical thickness of aerosol results in higher intensities of scattered thermal radiation,[1] and in expansion of the region within which the adjacency effect forms via both single and multiple collisions. However, starting with certain values of τ_{sct} (e.g., for maritime aerosol, λ = 3.75 μm, $S_M < 3$–5 km) for single scattering (it dominates in the structure of the flux of scattered radiation) further growth of the optical thickness results in lower J^{SS}_{surf}, and respectively in a decrease of the radius of lateral illumination (Fig. 2*b*). Simultaneously, J^{MS}_{surf} increases and the relative contribution from the atmosphere into the flux of scattered radiation increases as well. As a result, saturation of radius of lateral illumination takes place.

3. A dominating (more than 60%) contribution to the intensity of lateral illumination comes from a surface area within the radius R = 1 km about the sighting point. The contribution from remote areas quickly falls off with the range from the sighting point, as illustrated by the function $F(r)$ (Fig. 3). Such a dependence prevails through the considered range of optical and geometric observational conditions. The relative contribution from an area of 1 km in radius normally increases as the level of atmospheric turbidity increases (Fig. 3). It is only for maritime aerosol at λ = 3.75 μm and $S_M < 3$–5 km that the value of $F(r)\big|_{r=1}$ starts to fall at lower visibilities. The explanation of that fact may be found in point 2 of the above analysis.

4. Qualitatively, the dependence of the radius of lateral illumination on the optical thickness of atmospheric aerosol, including the tendency of R to saturate, is typical for all the considered types of aerosol. However, noticeable differences between these radii from one aerosol type to another at a fixed value of τ_{sct} make it possible to assume that, apart from τ_{sct} the value of R is affected by the single scattering albedo and by the scattering phase function.

It is of practical interest to compare the lateral illumination radius and the spatial resolution (SR) of several systems of satellite remote sensing, namely, AVHRR (sea surface sensing, λ = 3.75 and 10.8 μm, SR ≃ 1 km, Ref. 3) and HCMR and MSU–SK (land surface sensing, λ ≃ 11 μm, SR ≃ 1 km, Refs. 3,4).

Analyzing the obtained data in this context one may note the following:

In case of maritime aerosol the radius of lateral illumination exceeds SR ≈ 1 km for:

the level $\delta T_\lambda \simeq 1°$ at $S_M < 20$–30 km (λ = 3.75 μm) and $S_M < 11$–17 km (λ = 10.8 μm);

the level $\delta T_\lambda \simeq 0.5°$ at $S_M < 35$–50 km (λ = 3.75 μm) and $S_M < 21$–31 km (λ = 10.8 μm).

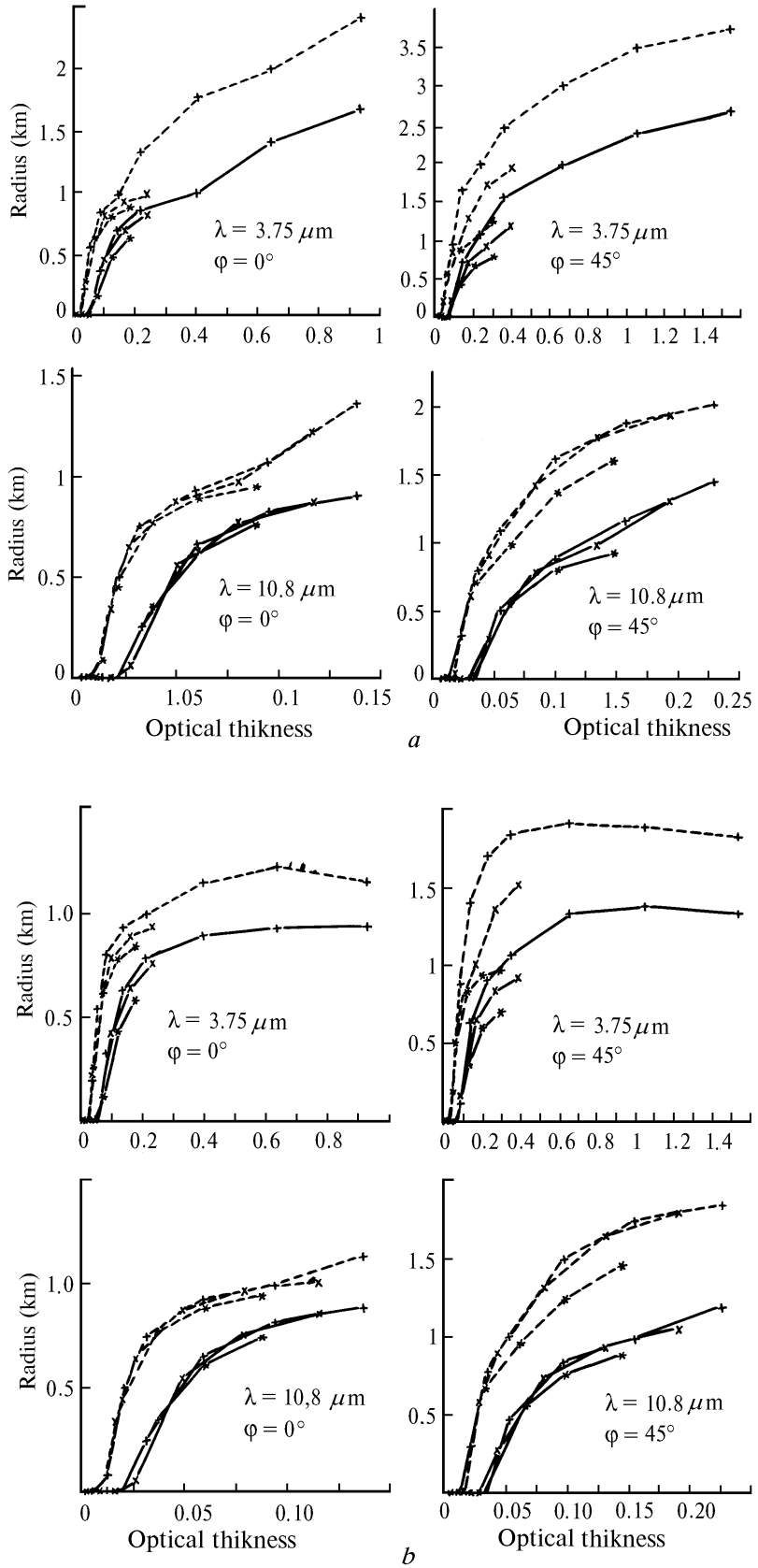

Fig. 2. Lateral illumination radius vs. optical thickness of aerosol scattering (midlatitudinal summer) for rural (x), maritime (+), and urban aerosol (∗). Single scattering (a) and multiple scattering (b).

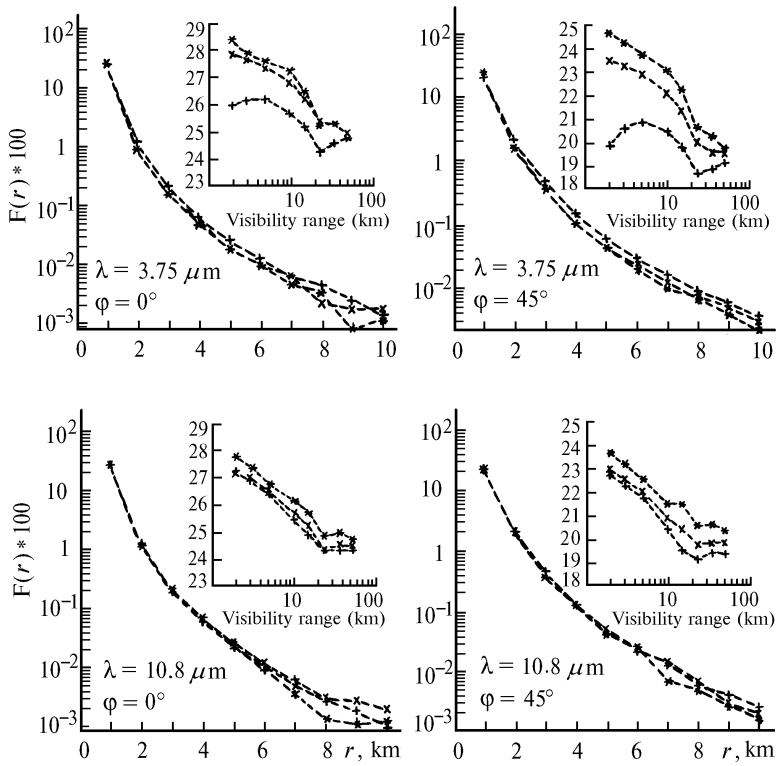

Fig. 3.Relative contribution of elements of the surface F(r) to the intensity of lateral illumination vs. range from the point of sensing and the dependence of $F(r)\Big|_{r=1}$ *on the visibility range ((midlatitudinal summer) for rural* (x), *maritime* (+), *and urban aerosol* (∗).

In cases of rural and urban aerosols the radius of lateral illumination R exceeds SR ≃ 0.5 km for:

the level $\delta T_\lambda \simeq 1°$ at $S_M < 7–12$ km ($\lambda = 3.75$ μm) and $S_M < 11–16$ km ($\lambda = 10.8$ μm);

the level $\delta T_\lambda \simeq 0.5°$at $S_M < 16–22$ km ($\lambda = 3.75$ μm) and $S_M < 20–28$ km ($\lambda = 10.8$ μm).

Summarizing the above we drew the following conclusions:

1. Even under high requirements on the accuracy, $\delta T_\lambda \approx 0.1°$ of the computed radiative temperature of free radiation of the A–US system the radius of the effective range of lateral illumination does not exceed 9 km for any model considered.

2. In case the accuracy of remote sensing of the surface temperature is on the order of 0.5–1°, the effective size of area, within which the lateral limitation is formed, exceeds the linear size of instant sighting field of systems for remote IR sensing of underlying surface of middle and high spatial resolution (less than 0.5–1 km) for the majority of optical and meteorological situations. This fact must be taken into account when interpreting results of remote sensing of such underlying surfaces which are characterized by significant temperature inhomogeneities outside the field of view of a sensing system.

REFERENCES

1. S.V. Afonin, V.V. Belov, and I.Yu. Macushkina, Atmos. Oceanic Opt. **7**, No. 6, 423–429 (1994).
2. J. Otterman and R.S. Fraser, Appl. Opt. **18**, No. 16, 2852–2860 (1979).
3. Ph.N. Slater, Remote Sensing of Environment, No. 17, 85–102 (1985).
4. A.S. Selivanov and Yu.M. Tuchin, Studies of Earth from Outer Space, No. 3, 101–106 (1988).